Field-Effect Flow Control for 2-D and 3-D Microfluidics

(February 13, 2006)

Sponsored by

Defense Advanced Research Projects Agency (DOD)
(Controlling DARPA Office)

ARPA Order Nr. P641/08

Issued by U.S. Army Aviation and Missile Command Under

Contract No. DAAH01-03-C-R182

Ponniah Sivanesan, Ph.D., Principal Investigator
Calibrant Biosystems
910 Clopper Road, Suite 220N
Gaithersburg, MD 20878
301.977.7900 (voice)
301.977.7981 (fax)

Effective Date of Contract: 04/22/03

Contract Expiration Date: 01/29/06

Short Title of Work: Final Report

Reporting Period: 04/22/03 – 01/29/06

Calibrant Biosystems, Inc.
910 Clopper Road, Suite 220N
Gaithersburg, MD20878

DARPA/DSO

REPORT DOCUMENTATION PAGE

Form Approved
OMB No. 0704-0188

1. REPORT DATE *(DD-MM-YYYY)*	2. REPORT TYPE	3. DATES COVERED *(From - To)*
13/02/2006	Final Technical Report	04/22/03- 01/29/06

4. TITLE AND SUBTITLE
Field-effect flow control for 2-D and 3-D microfluidics

5a. CONTRACT NUMBER
DAAH01-03-C-R182

5b. GRANT NUMBER

5c. PROGRAM ELEMENT NUMBER

6. AUTHOR(S)
Sivanesan, Ponniah

5d. PROJECT NUMBER
RTW81 05

5e. TASK NUMBER

5f. WORK UNIT NUMBER

7. PERFORMING ORGANIZATION NAME(S) AND ADDRESS(ES)
Calibrant Biosystems, Inc. 910 Clopper Road, Suite 220N Gaithersburg, MD 20878

8. PERFORMING ORGANIZATION REPORT NUMBER
DAR/4.2/2003

9. SPONSORING / MONITORING AGENCY NAME(S) AND ADDRESS(ES)
US ARMY AVIATION & MISSILE COMMAND REDSTONE ARSENAL AL 35898-5280

10. SPONSOR/MONITOR'S ACRONYM(S)

11. SPONSOR/MONITOR'S REPORT NUMBER(S)

12. DISTRIBUTION / AVAILABILITY STATEMENT
Approved for public release; distribution unlimited.

13. SUPPLEMENTARY NOTES

14. ABSTRACT

Report prepared for the SBIR Phase II contract titled "Field-effect flow control for 2-D and 3-D microfluidics". The SBIR Phase II project reported here proposed to develop technology for *Multidimensional Separations and Mass Spectrometry in a Microfluidic System*. This system combines the field-effect flow control technology with a related microfluidic product developed at Calibrant for proteomic analysis, the MicroDisplay2D. The multidimensional separation in a microfluidic platform is designed to enable multianalyte pathogen detection using protein biomarkers for effective, portable, and universal biological warfare agent identification. The work was focused on optimization, integration, and validation of the combined platform. The end goal was to develop a high resolution two-dimensional separation microfluidic platform that could rival 2D-PAGE in capability for producing protein expression maps. The initial target application was to utilize protein expression maps produced from this technology to identify protein biomarkers unique to specific pathogens of concern that can be employed as biological warfare agents.

15. SUBJECT TERMS
SBIR Report, Microfluidics, Flow control, Field-effect, Pathogen, Biological

16. SECURITY CLASSIFICATION OF:			17. LIMITATION OF ABSTRACT	18. NUMBER OF PAGES	19a. NAME OF RESPONSIBLE PERSON
a. REPORT	b. ABSTRACT	c. THIS PAGE			Don L. Devoe
U	U	U	UU	20	19b. TELEPHONE NUMBER *(include area code)* (301) 977 7900 x 12

Project Summary

The SBIR Phase II project reported here proposed to develop a technology for *Multidimensional Separations and Mass Spectrometry in a Microfluidic System (MS^3)*. The MS^3 system combines the FEFC technology developed in the Phase I SBIR effort with a related microfluidic product developed at Calibrant for proteomic analysis, the MicroDisplay2D. The MS^3 platform is designed to enable multianalyte pathogen detection using protein biomarkers for effective, portable, and universal biological warfare agents (BWA) identification.

The work was focused on optimization, integration, and validation of the combined platform. The end goal was to develop a high resolution two-dimensional separation microfluidic platform that could rival 2D-PAGE in capability for producing protein expression maps (PEMs) while doing so much more rapidly and reproducibly. The initial target application was to utilize PEMs produced from this technology to identify protein biomarkers unique to specific pathogens of concern that can be employed as biological warfare agents.

Phase II work plan consisted of four primary tasks:

Task 1 – FEFC optimization
Task 2 – MicroDisplay2D optimization
Task 3 – MS^3 instrument development and automation
Task 4 – System demonstration

An overview of the achievements during the Phase II effort of this SBIR project is described in this report.

Task 1– FEFC Optimization

The FEFC technology developed in Phase I was demonstrated to be capable of transferring a sample volume from a planar microchannel into a 3rd dimension microchannel by inducing pressure-driven flow through the 3-D channel. Work has been done to optimize the amount of sample volume that can be transferred to the third dimension microchannel network with a goal of achieving 75% transfer efficiency. The test devices with 3-D channels were fabricated in PDMS polymer (Figure 1a & 1b) and the pumping efficiency tests were conducted using a particle tracking method.

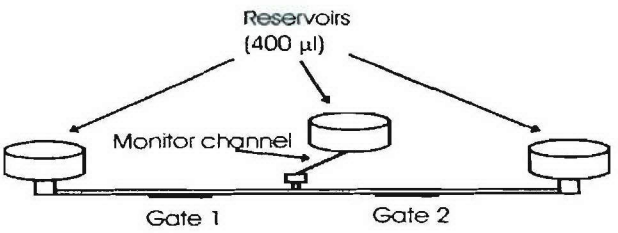

(a)

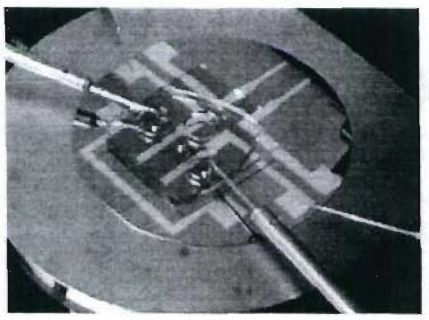

(b)

Figure 1. (a) Schematic diagram of the microfluidic test device with monitor channel for easy imaging process (b) a fully assembled test device on a RF-1 probe station stage.

The hydraulic pumping efficiency of the FEFC method was measured using a device with a monitor channel length of 0.4mm in order to achieve a higher pumping efficiency while having enough channel length to measure flow velocity using the particle tracking method. Monitor channels shorter than 0.4mm could not be clearly imaged for velocity measurements due to optical noise and difficulties associated with selecting individual beads and sequentially imaging them in a short channel length before they are lost to the reservoirs. For a gate voltage of 100Volts, the flow rate in the monitor channel was measured and compared with the flow rate in the main channel. The flow rate in the monitor channel was 58.1% of that in the main channel when the gate voltage is applied. Figure 2 shows the experimentally achieved efficiency and the projected efficiency for this microchannel device at the breakdown voltage for a 1µm-thick Parylene C layer.

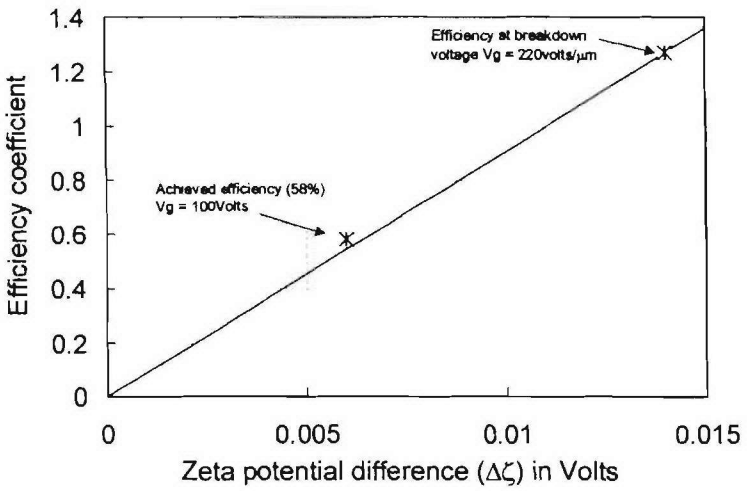

Figure 2. Volume transfer efficiency for hydraulic pumping versus the zeta potential difference for the tested device.

These results illustrate how the hydraulic pumping efficiency of this microfluidic device can be improved with higher gate voltages. The breakdown limit shown in Figure 2 is based on the theoretical values. In practice, for a given thickness of the Parylene layer, electrical breakdown occurs before the voltage reaches the theoretical limit. This results from a lack of uniformity in the electric field density across the electrode, which is often very high at the electrode edges. Patterning electrodes smooth edges and depositing a layer of Parylene C with uniform thickness are essential for reaching the theoretical breakdown point. Other factors such as the pH of the buffer solution and the electrode position are also parameters of interest for future investigation to enhance the pumping efficiency in EO micropumps.

Task 2 – MicroDisplay2D Optimization

Task 2.1 Microfluidic System Fabrication

Autofluorescence from the substrate material at the excitation wavelength is one of the main factors determining the signal to noise ratio of the optical detection system. Consequently, the autofluorescent properties of a variety of polymer substrate materials were investigated to determine the material that was most amenable to the laser-induced fluorescence detection employed in this project. Different polymer samples were obtained from different companies and are listed in Table 1 below.

Table 1. Polymer substrate materials and their visible transmission percentages

Polymer type	Vendor	Specified percentage of visible light transmission
1020R	Zeon Chemicals, KY	92
1060R2t	Zeon Chemicals, KY	92
E48R2t	Zeon Chemicals, KY	92
4802t	Zeon Chemicals, KY	92
Fosta-tek ADC	Fosta-tek Optics, MA	92
PMMA	Piedmont Plastics, MD	91
PC	Piedmont Plastics, MD	89

Autofluorescence from each of these samples having almost equal thickness were measured at an excitation light wavelength of 488nm and compared. Figure 3 below shows the measured values for each polymer. Polycarbonate (PC) substrates show the highest autofluorescence among the tested materials. While the autofluorescence values for 1060R2t, 1020R and E48R2t polymers (all cyclic olefin copolymer derivatives) from Zeon chemicals are comparable to polymethyl methacrylate (PMMA) from Piedmont Plastics, the cost for the former is much higher than PMMA polymer. As result, PMMA was selected as the best material to utilize for the development project.

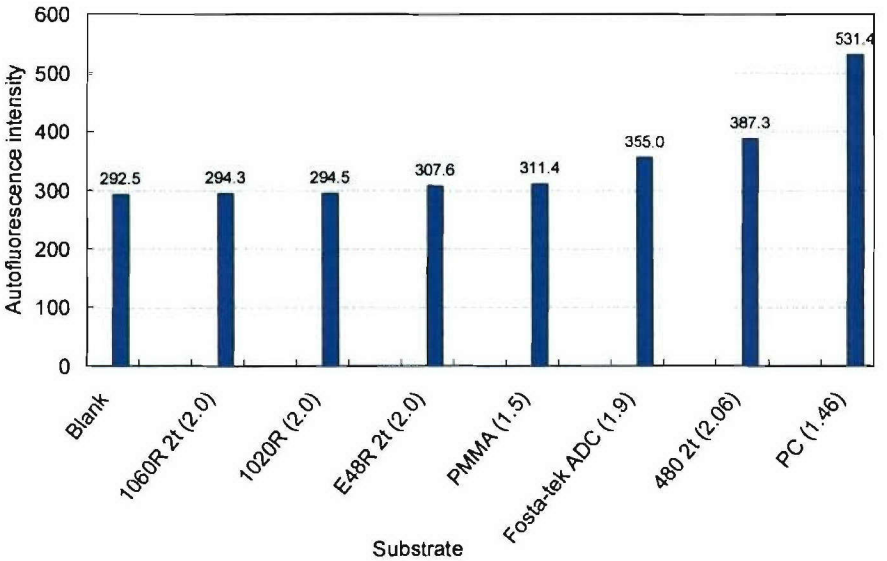

Figure 3. Autofluorescence measured in different types of polymer materials. Thickness of each sample is listed within the brackets. Units are in millimeters.

Once the optimal polymer substrate material was identified, embossing and bonding procedures previously demonstrated were initially used to imprint and bond microfluidic chips using SU8 as the template material and silicon wafers as the substrate material. SU8

is a lithographically-patternable polymer which offers the important benefit of reducing the fabrication cycle time from 1-2 days per template, to 1 hour per template, enabling significantly more design variations to be explored in the project. However, difficulties arose in embossing plastic substrates with SU-8 templates when moving to high-density microfluidic network designs containing the target 128 second dimension channels as outlined in the proposal. The tremendous frictional force present when removing the template from the embossed plastic substrate almost always overcame the adhesion of the SU-8 pattern to the silicon wafer. As a result, the bond between the SU-8 and silicon would fail with much of the SU-8 left imbedded in the microfluidic channels rendering the devices unusable. After significant effort was exerted to resolve this deficiency with the SU-8 templates, the decision was made to switch to using wet-etched silicon templates for fabrication of the high-density devices.

After optimizing the embossing procedure for high-density microfluidic devices using the wet-etched silicon templates, efforts were made toward optimizing the bonding of embossed substrates with coverpieces to enclose the channels. Because the time associated with preparing a device for analysis must be included in the total analysis cycle time, initial filling and interface establishment must be performed under high pressures in order to minimize time allocated to chip preparation. One factor that determines the chip filling time and, therefore, the test time is the bond strength of the device. Even when optimized, thermal bonding of the high channel density devices was not robust enough. While the mechanical bond strength of thermally bonded PMMA devices is sufficient for slow, low-pressure filling of the microfluidic chips, it is not adequate for a desired high-pressure filling process that is capable of loading aqueous and gel solutions into the entire microfluidic network much more rapidly. The reduced binding area resulting from the increase in channels combined with the relatively low strength of thermal bonding produced devices that were prone to delamination while being filled with gel solutions under high pressure. As a result, efforts were redirected towards improving the mechanical strength of the microfluidic device by replacing the thermal bonding process with a solvent bonding method. In the solvent bonding method, Ethylene dichloride is evaporated at room temperature onto a PMMA coverpiece. Following the evaporation step, an imprinted PMMA substrate is brought into contact with the solvent-treated PMMA under low force to bond the pieces together. During the process, the imprinted PMMA is arranged so that its channel network becomes enclosed by the solvent-treated PMMA coverpiece. Since the surfaces of the two PMMA substrates are chemically fused due to the partial solvation of the PMMA coverpiece, devices produced from this process are much stronger than those produced by thermal bonding. Unlike thermal bonding, solvent bonding does not require long contact times, high temperatures, or high forces to achieve effective bonding. We have developed a method to effectively perform solvent bonding utilizing a cold press at room temperature. The bonding strength and quality has been found to depend on parameters such as evaporation time, contact force, and duration. Experimental results show that high-quality bonding of 2D microfluidic devices can be achieved by using a 4-minute solvent evaporation time in conjunction with application of 4500 lbs of force in a cold press for 2-3 minutes.

Task 2.2 Laser-Induced Fluorescence Detection (LIFD) and Imaging

In order to achieve the detection sensitivity required to produce the powerful PEM images pursued in this project, several iterations of the optical detection system were developed. The previous version of the detection system (Figure 4) used the 488-nm output of a 200-mW Argon-Ion laser as the excitation light source for performing LIFD. The primary disadvantage of this approach stems from the need for large format optics to image the entire second-dimension microchannel array in a simultaneous manner. This optical configuration produces a relatively low numerical aperture value resulting in low collection efficiency of emitted fluorescence from the channels. In addition, the optically generated laser line format retains the Gaussian profile of the incident laser beam source resulting in a nonuniform excitation power across the microchannel array with the center channels receiving the most photons and the channels at the edge receiving the least. This results in an order-of-magnitude higher detection sensitivity in the center of the array versus the edges.

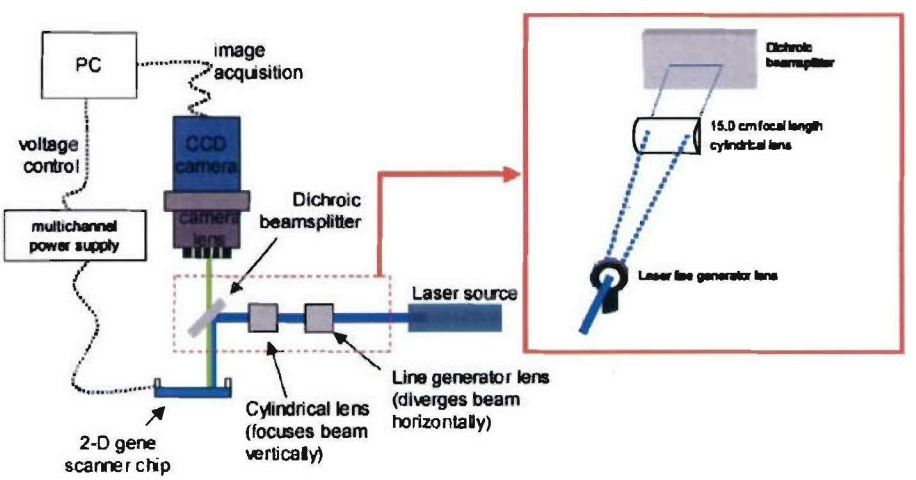

Figure 4. A schematic of the previous optical system using a laser excitation source.

To overcome the disadvantages of the first detection scheme, the optical system was redesigned to increase the excitation and collection efficiencies to the levels required to detect relatively low abundance proteins at the end of the two-dimensional separation. The finalized version of the LIFD system utilizes a custom scanning objective lens and detector combination for exciting fluorophores and effectively collecting fluorescence in the absence of any bias toward channel position across the 2nd dimension channel array. A schematic of the detection system is shown in Figure 5 below. The excitation source is a laser that is fixed at a position off of the scanning stage. The laser beam is directed into a filter cube where a dichroic beamsplitter is positioned at a 45-degree angle of incidence to the laser. The dichroic beamsplitter reflects the laser beam up through a high numerical aperture microscope objective lens, which focuses the beam onto the microchannel while at the same time collecting the fluorescence emission. The emission light collected by the objective lens is collimated and transmitted through the dichroic beamsplitter where the

photons are detected by a photomultiplier tube (PMT). A longpass emission filter and a rugate notch filter are placed at the orifice of the PMT to reject laser scatter.

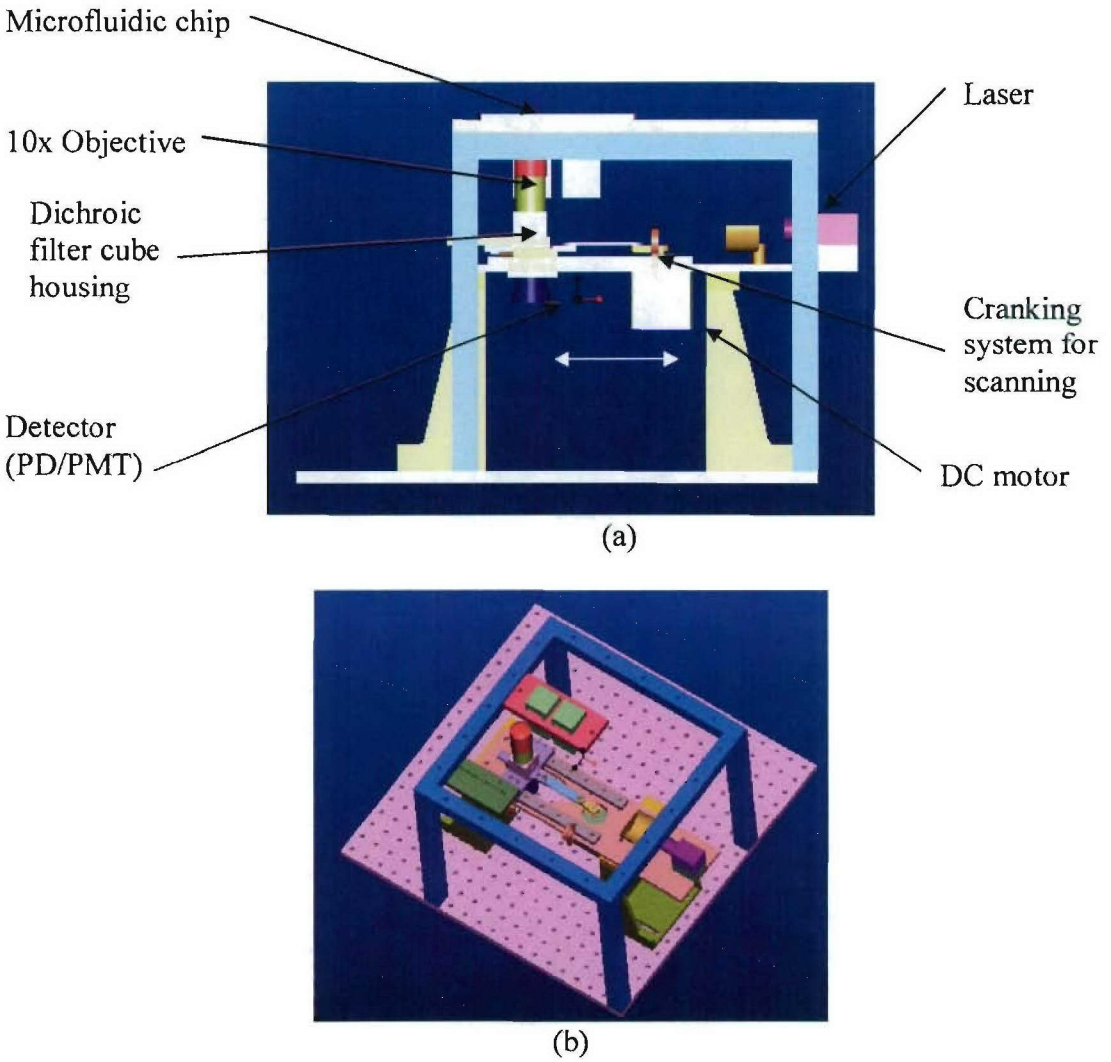

Figure 5. Schematic of the final optical scanning system for fluorescence detection (a) side view and (b) a top view with top mounting plate removed.

The linear scanning of the optical assembly is achieved by a cranking action using a DC motor and throwing arms. In order to minimize the vibration effects during the scanning operation, the entire scanning parts are firmly secured to the base plate by means of two angle brackets. The optical assembly is scanned across the entire second dimension array (4.5cm) at a frequency of 5 Hz. Fluorescence emission is recorded by the PMT at a rate of 4.5 kHz resulting in a spatial excitation resolution of 100 μm per detector scan. By synchronizing the motor with the detector, the instantaneous laser position can be mapped to each emission scan. This enables the time domain in the fluorescence data recorded for each optical scan to be converted to a spatial domain. Custom imaging software developed

for this application is then used to convert each data point to a pixel array and a pseudo gel-like image of the two dimensional separation is produced. The sensitivity of this system provides detection of proteins labeled by SYPRO red down to concentrations of 1μg/ml.

Task 2.3 Optimization of 2-D Protein Separation in High-Density Microchannel Network

Initial attempts to improve upon the comprehensive 2-D separation of *E. coli* cell lysates in a 128-channel device were unsuccessful. As a result, subsequent efforts were focused on a scaled-down 32-channel network design (Figure 6) that was identical in every way to the 128-channel device except for the density of the second-dimension channel array. The design of the ten-channel proof-of-concept network was an ideal model because each microchannel in the network terminates at an individual point allowing for each channel to be electrically and fluidically isolated. In such a design, the fluid and electrical dynamics of the system can be easily predicted. However, the foremost issue that must be considered when expanding the channel density of the microfluidic network is fluid and electrical control access of the microchannels from the external environment of the device. When dealing with a network density of 128 channels, the logistics involved in performing separations in such a network requires the channels to have some degree of interconnectedness in order to minimize the number of electrical and fluid access points needed to perform a separation. However, while this channel interconnectedness simplifies the logistics of controlling the separation process, it significantly increases the complexity and dynamics of the microchannel network by introducing several alternative fluid flow and electrical circuit paths within the network.

To characterize the fluid and electrical dynamics within and optimize the interconnected network design, an electrical equivalent circuit model of the 2-D chip was developed and analyzed using Pspice software. Analysis of the electrical equivalent circuit model focused on what were identified as the two most important aspects: current leakage to the second dimension channels during isoelectric focusing in the first dimension channel; and the electric field distribution during gel electrophoresis in the second dimension channels.

The original design as analyzed has an interconnected fluidic network on the top and the bottom of the separation channels (Figure 6). Interconnected second dimension channels and a half period relative spatial shift of the second dimension channels above and below the isoelectric focusing (IEF) channel (E9 - E10 in Figure 6) resulted in increased current leakage from the IEF channel and a non-uniform electric field distribution in the second dimension separation channels. Initially, the lengths of different groups of channels were varied to minimize the amount of current leakage to the side channels when an electrical potential is applied across the IEF channel (E9 –E10). The results showed very small change in current leakage even for a 100% change in second dimension channel length. This was due to the interconnected grouping of channels and the difference in resistivity between the separation medium present in the IEF channel (aqueous buffer) and the second dimension channels (gel). Therefore, the effect on IEF current leakage when isolating different group of channels with separate reservoirs was investigated.

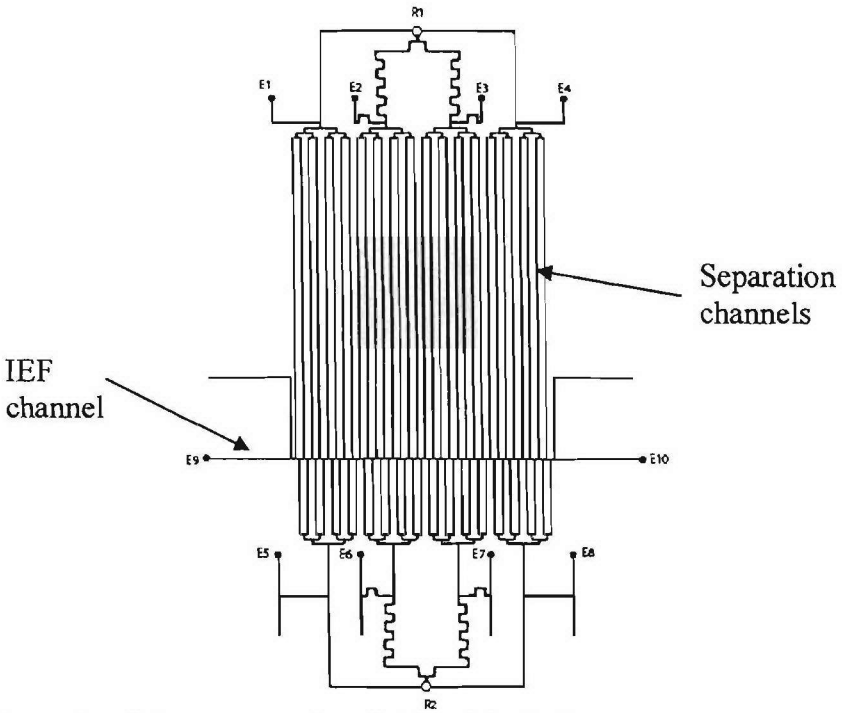

Figure 6. Schematic of the current microfluidic chip design.

The 32-channel second dimension network was grouped into four, eight and sixteen different channel groups with each group having separate fluid/electrical access port. For example, Figure 7 shows a schematic of four groups of channels with four separate reservoirs.

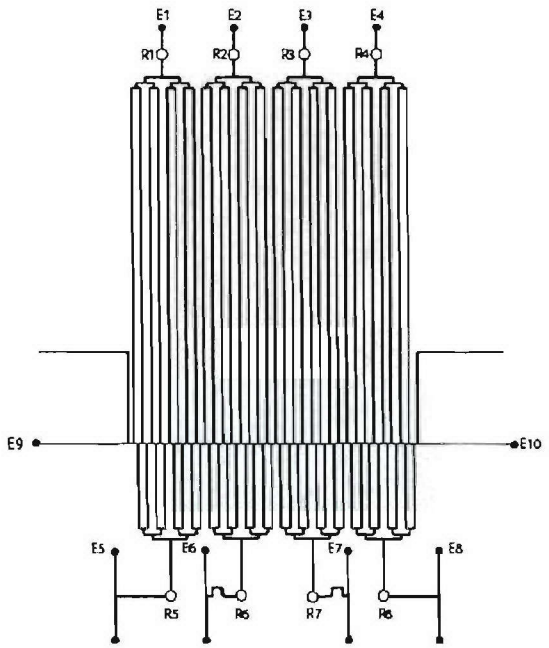

Figure 7. Schematic of 4 reservoir design (○– liquid reservoirs; ●- electrode reservoirs).

Total IEF current leakage was estimated for four, eight and sixteen reservoir configurations and compared with the estimated value for the current leakage in the existing configuration. The results are given in Table 2 below.

Table 2. Percentage of total current leakage in 4, 8, and 16 reservoir configurations.

Percentage of total IEF current leakage to the second dimension channels							
Current (one reservoir) configuration		4 reservoir configuration		8 reservoir configuration		16 reservoir configuration	
Before IEF	After IEF	Before IEF	After IEF	Before IEF	After IEF	Before IEF	After IEF
69	95	35	77	13.5	44	6	24

It should be noted that the resistivity of the first dimension channel (IEF channel) increases as the IEF separation proceeds and, hence, we should expect an increase in current leakage upon completion of the IEF separation. Results plotted as percentage of total current leakage along the IEF channel in Figure 6 for the circuit model show this expected increase in current leakage after the focusing process is completed. The results in Fig. 8 were obtained for an equivalent circuit of the microfluidic network shown in Fig. 6.

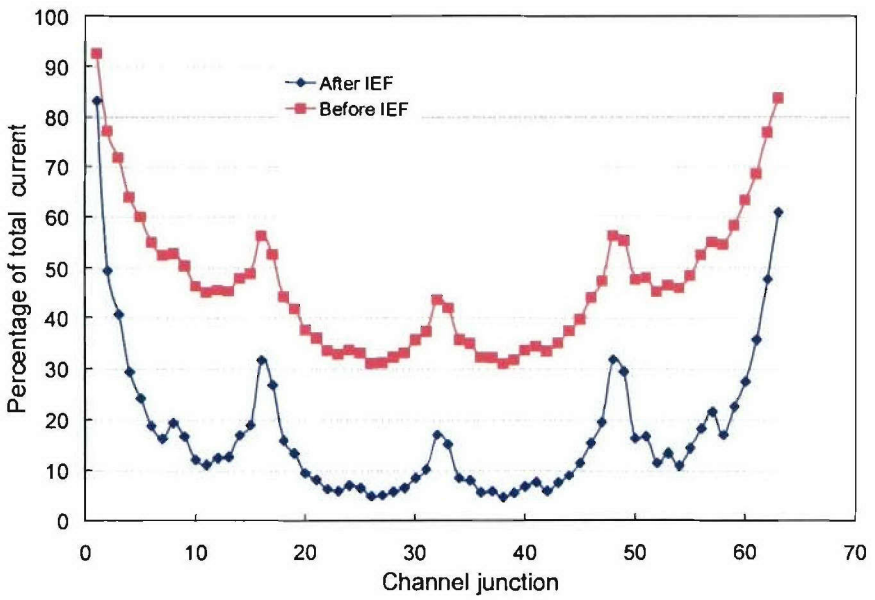

Figure 8. Total IEF current flow before and after IEF along the IEF channel estimated using equivalent circuit analysis for the design in Figure 4.

Results in Table 2 show that the IEF current leakage can be significantly reduced by increasing the number of reservoirs that connect the second dimension channels. This is expected as increasing the number of reservoirs connecting the second dimension channels approached the ideal design model employed in the proof-of-concept phase. However, the target footprint size of the device made it possible to accommodate only a chip design with 8 reservoir configuration. With the use of an eight-reservoir chip design, total IEF current leakage at the onset of IEF process can be reduced to about 14% compared to a 70% leakage in the initial chip design.

Second, the electric field distribution in the second dimension channels was investigated using the same equivalent circuit model. Electric field for the gel electrophoresis in the second dimension channels is provided by applying a potential between electrical ports E1-E4 and E4-E8 (Fig. 6). The electric field distribution in the separation channels was calculated using the equivalent circuit model. The percentage of electric field variation from one end to the other is approximately 16%. This variation in electric field strength across the 32 separation channels can be attributed to the spatial shift of the top second dimension channel network with respect to the bottom second dimension channel network along the IEF channels. Note that this spatial shift is necessary for complete transfer of focused protein in the IEF channel into the second dimension channels. In order to compensate the non-uniform electric field in separation channels due to this spatial shift, two extra long channels at the ends of the IEF channel were included in the design to provide balance. An optimization analysis was performed to determine the required lengths of these channels to produce a uniform electric field in all 32 separation channels. After the two extra channels were included, the variation in electric field was nearly eliminated as shown (red squares) in Figure 9.

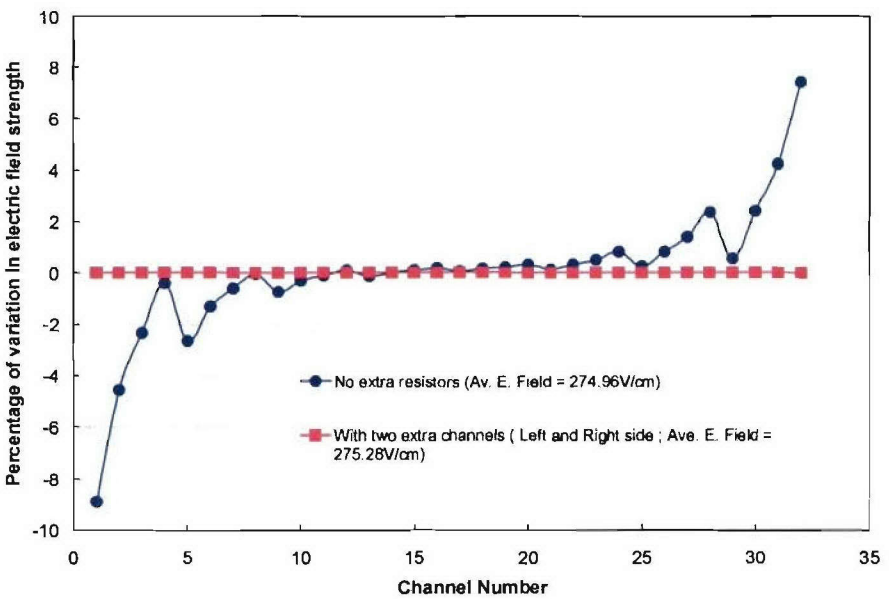

Figure 9. Simulation results for the electric field strengths in the second dimension channels before and after design modification.

Note that the average electric field in the second dimension channels had little change after the introduction of extra side channels while the uniformity of electric field strength has improved significantly. Based on the results from the circuit model analysis, an optimized interconnected network design (Fig. 10) for the 2D microfluidic chip was identified and employed for the remainder of the project.

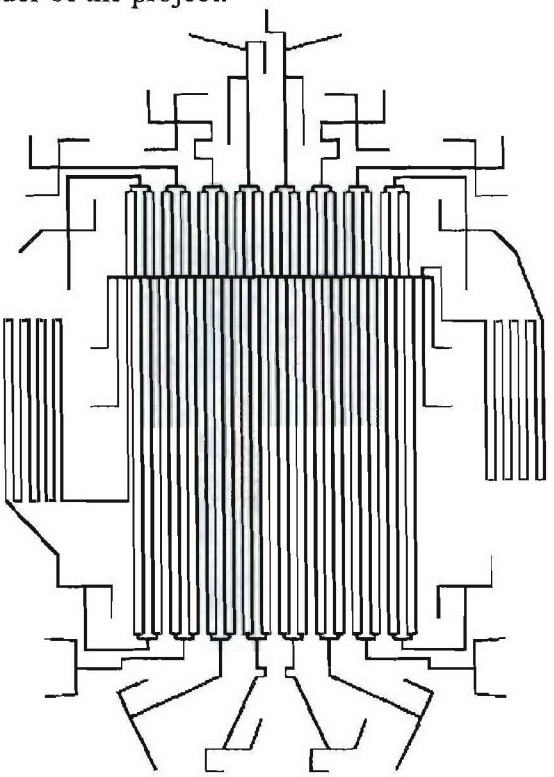

Figure 10. New chip design with two extra side channels and 8 reservoirs at the top and bottom of the second dimension of the channels.

As demonstrated in the proof-of-concept development of this technology outlined in the original proposal, it is necessary to establish an aqueous/gel interface boundary between the first dimension IEF channel and the second dimension parallel gel electrophoresis channels in order to achieve optimal separation. Upon commencement of the project, it was determined that the relatively complex manual procedure required to prepare the microfluidic device and establish the necessary gel/aqueous interface for running the two dimensional separation was too time-consuming to enable the realization of two crucial project milestones: (1) achieving a complete 2-D protein separation in under 15 min; and (2) completing a full analysis cycle in less than 15 min under manual operation. To address this, an effort was made (in parallel to Task 2 efforts focused on separation optimization) to automate the operation of the full analysis cycle with the goal of reducing the total cycle time to 15 minutes.

Task 3 – Instrument development and automation

Custom software and hardware were developed to provide control for all components in the system making the process fully automated. A manifold system with on-board actuated valving was developed to provide streamlined fluidic and electrical interfacing with the 2-D microfluidic device. Figure 11 shows an image of the core manifold substrate containing fluid distribution channels and valving access points. Figure 12 shows the manifold fully integrated into the instrument complete with valves for fluidic control.

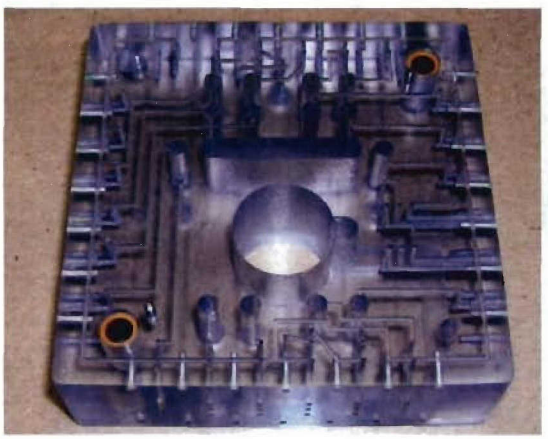

Figure 11. Image of core manifold substrate.

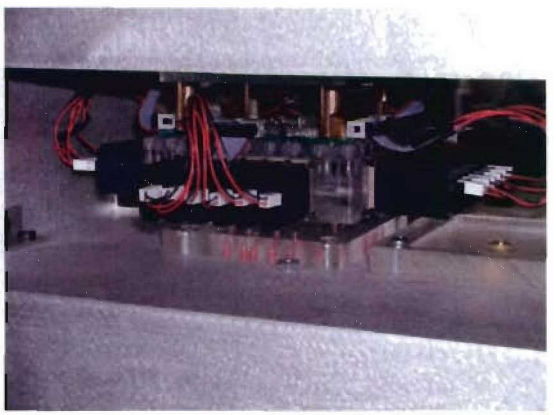

Figure 12. Image of fully-assembled manifold position in idle position over cleaning station.

Figure 13 below displays the model and the actual image of the overall instrument mechanical assembly.

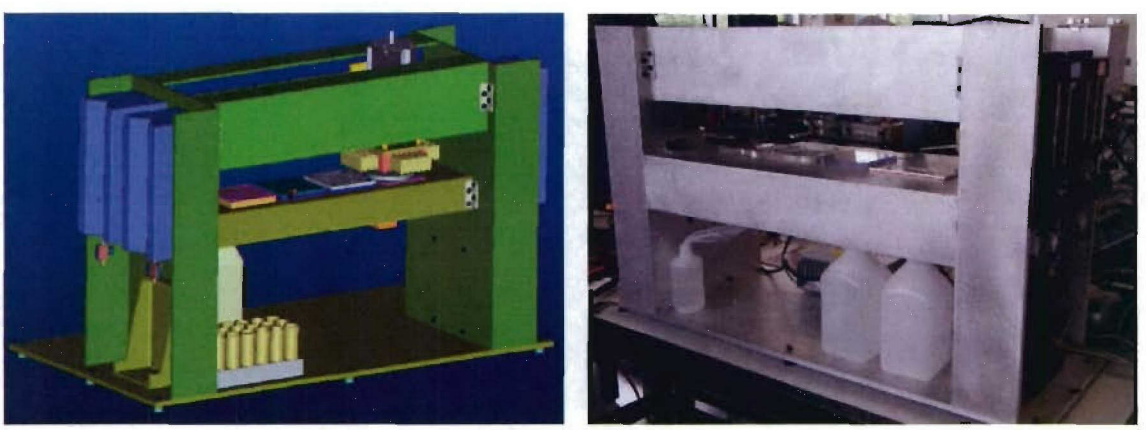

(a) (b)

Figure 13. (a) The 3D model and (b) the image of overall instrument assembly.

A custom integrated control scheme was prepared and provides automated operation of high voltage power supplies, manifold motion, syringe pumps, and fluorescence data collection and image processing. Figure 14 below shows the flow chart of the entire control scheme for the system. Figure 15 displays a screenshot of the custom Labview-based software used to operate the system.

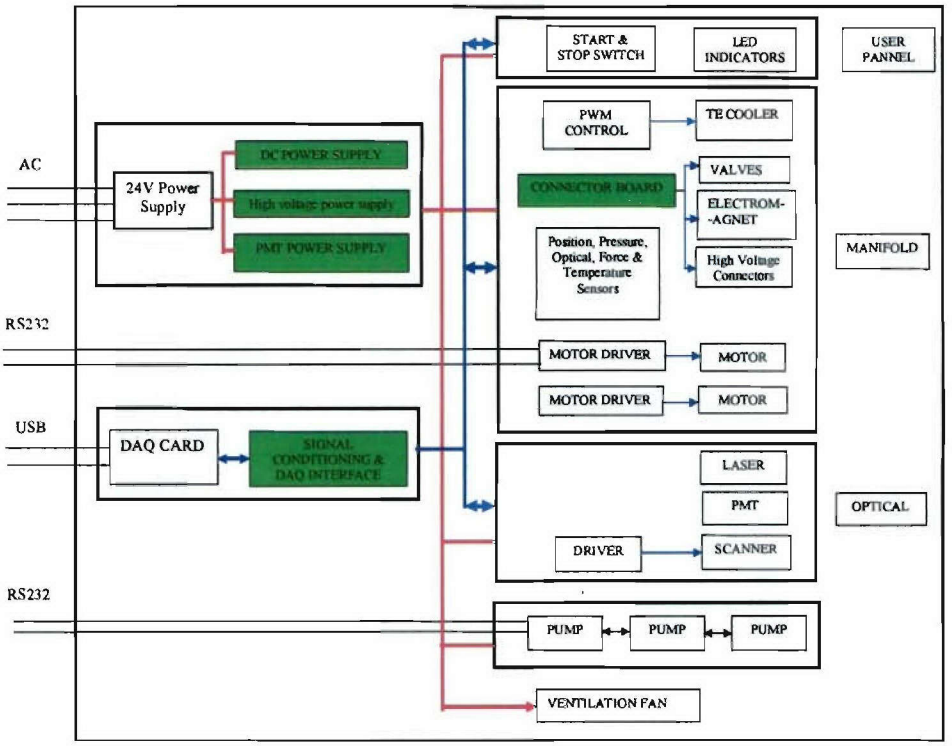

Figure 14. Flow chart showing the controls and hardware for the MS^3 system for pathogen detection.

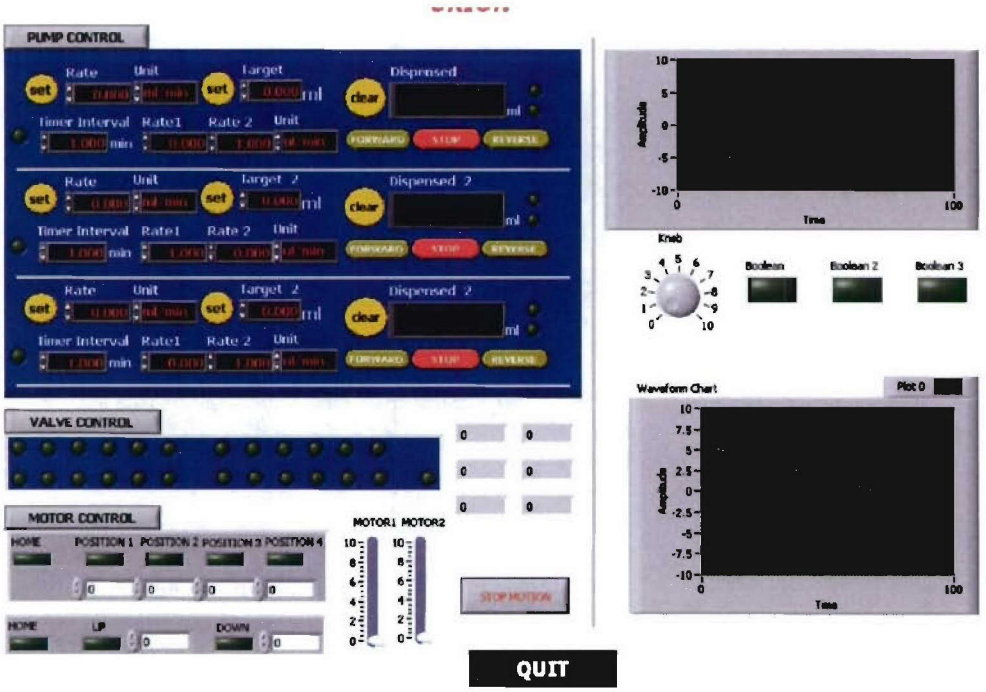

Figure 15. Screenshot for control software.

Once automation and system-level controls were developed, efforts were focused on establishing a consistent and repeatable aqueous/gel interface between the first and the second dimension channels. This work is crucial for reducing run-to-run variability in the performance of the 2D on-chip separations. Multiple tests were performed to study the extent to which a high-quality 1D-2D/aqueous-gel interface, necessary for achieving high-resolution separations, can be established in a repeatable manner. The reproducibility study focused on both variations during multiple uses of a single device and on variations occurring between multiple devices.

The variations were measured in two ways. First, the flow rates used to establish a high-quality interface were recorded. In all tests, there were no variations in these flow rates across multiple tests on a single device. However, small variations in required flow rates occurred between devices with the ratios of the three input flow rates ranging from 1:1:1 to 1:1.2:1.4. Second, the position and size characteristics of protein bands separated by isoelectric focusing (IEF) following establishment of the 1D-2D interface were studied. In all cases, upon establishment of a high-quality interface, IEF separations produced repeatable results. A CCD image of a section of a typical interface is shown in Figure 16.

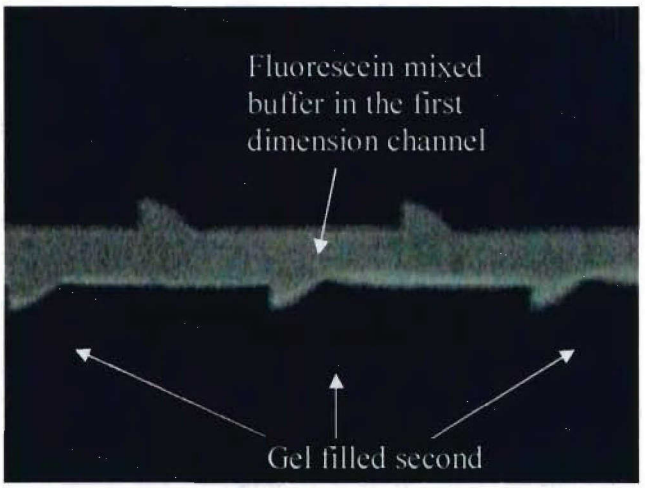

Figure 16. A section of chip at 20x magnification after establishing interface between buffer (containing fluorescein dye) in the first dimension channel and gel-filled second dimension channels.

Any variations in flow rates required to establish high-quality interfaces within different devices can be attributed to imperfect repeatability in the device fabrication process. It is expected that this variation will be minimized once the fabrication process is transferred to commercial injection molding.

Upon completion of the first dimension isoelectric focusing separation and subsequent protein band transfer to the parallel second dimension channel array, a high throughput parallel gel electrophoresis separation is performed to further separate focused proteins by size. The primary factor contributing to degradation of separation efficiency when performing electrophoresis separations is Joule (resistive) heating. As the temperature rises in the gel electrophoresis channel, the viscosity of the gel-sieving matrix is often decreased while at the same time analyte band diffusion increases. In a polymer microfluidic channel fabricated from a polycarbonate substrate, this phenomenon is even more significant as the thermal conductivity for polycarbonate is relatively low (0.2 W/m-K, 14.5% the value for fused silica), providing less than desired dissipation of the joule heating generated during a separation. Thus, during the Phase II development of this system, we have focused on integrating a TE cooling system into the base of the fluidic manifold to enhance the system capability for dissipating joule heating that is generated during the second dimension SDS-gel electrophoresis separation. In addition, the custom software developed for the MS^3 system has the ability to regulate the integrated TE cooling system to provide temperature control within the microchannels. This enables a constant and optimal temperature to be maintained in the microfluidic network resulting in enhanced separation reproducibility and performance.

In this effort, a custom TE cooling system was assembled using a multi-stage TE cooling module (Traverse City, MI), a thermally-conductive interface pad, a custom heatsink, and a fan. The TE cooling system was designed so that it does not obstruct the optical detection path or interfere with the fluidic interconnects when integrated into the manifold. With the

current setup, the maximum cooling capacity achievable at the surface of the TE cooling module is –20°C. In order to determine the actual temperature within the separation channels, extremely thin thermocouples (25-μm diameter) were inserted into three microchannels of the second-dimension channel array and fixed with epoxy in a manner so that the channels were not blocked. A separation voltage was applied to the second dimension channel array of the 2-D microfluidic separation platform to produce an electric field across the second dimension separation channels of ~200 V/cm. While holding the separation voltage constant, the cooling capacity (temp. at surface of TE cooling module) applied to the microfluidic channels by the TE cooling system was varied and held constant for 10-minute intervals and the subsequent temperature inside the channels was recorded by taking the average temperature in the three channels containing thermocouples once steady state was reached. Table 3 shows the significant effect the TE cooling system has on the temperature (and dissipation of Joule heating) in the microchannels.

Table 3. Effect of TE cooling capacity on microchannel temp.

E-Field, Separation (V/cm)	Cooling Capacity (Surface Temp, °C)	Channel Temp. (°C)
200	3.5	75.6
200	2.3	59.5
200	1.4	46.6
200	0.7	14.3
200	-0.4	12.6
200	-1.6	7.6

The effect of integration of the TE cooling system on the separation performance of the 2-D microfluidic separation system was assessed and showed promise for improving the reliability for the two-dimensional separation. After incorporating the TE cooling modifications into the 2-D microfluidic separation, a significant enhancement in detection sensitivity was achieved.

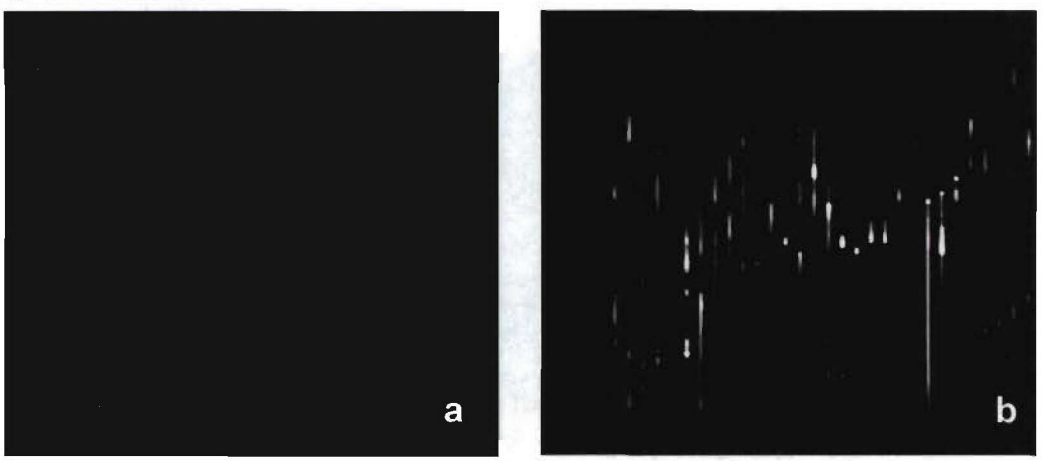

Figure 17. Gel-view image for 2-D microfluidic separation of *E. coli* cell lysates before (a) and after (b) system modifications.

To evaluate the performance of the optimized system prior to initiating Task 2, a large number (>30) of separations were attempted using *E. coli* cell lysate as a model system of moderate complexity similar that that expected for *H. pylori*. The detection sensitivity of the optimized system can be seen from the comparison of our best separation prior to optimization in Fig. 17a and our best separation results using the optimized system in Fig. 17b. Upon comparing the gel-view images for separations performed before and after the system modifications, it is readily apparent that the sensitivity of the system has been dramatically improved. Both separations were otherwise performed under identical conditions. The sample loading for the *E. coli* cell lysates in both cases was ~2 μL at a concentration of 0.5 mg/mL (total protein loading = 1 μg). Despite the observed improvement, repeatability among multiple tests was found to be poor, primarily due to variations in electrical and fluidic cross-talk between channels sharing a common reservoir, and variations in acid/base migration into the main IEF separation channel. Due to this problem, we believe the system requires additional development before being applied to comparative proteomic studies. This issue was identified near the end of the Phase II project, and modifications to the chip design were implemented in an attempt to improve our ability to perform effective IEF in the coupled microfluidic system. A schematic of the modified low-density chip design with 10 second-dimension channels is shown in Fig. 18(a), with a photograph of a fabricated device in Fig. 18(b).

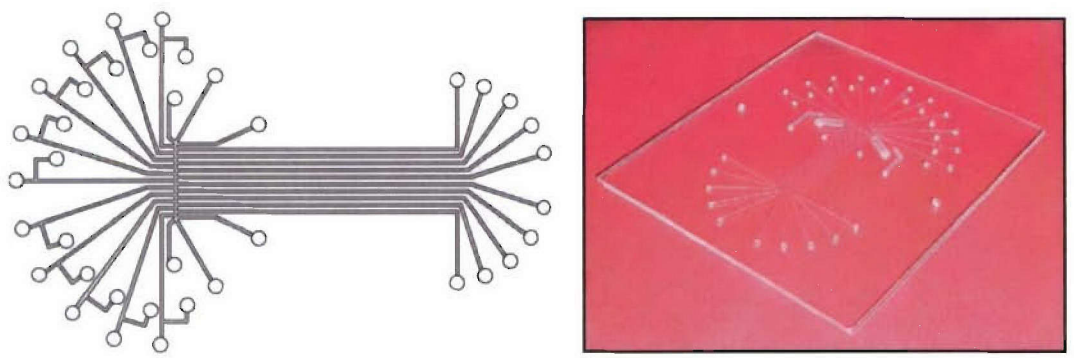

(a) (b)

Figure 18. Modified design of a 10-channel 2-D protein separation chip.

Key features of this new design include complete fluidic isolation for each second-dimension channel, and modifications to the position of the acid and base reservoirs to provide more effective establishment of the pH gradient during IEF. This design is currently being tested, together with testing using a variety of simple 1-D separation channels with modified channel and reservoir geometries to reduce variability. Initial results indicate substantial improvements by using reservoirs connected to the IEF channel by wide and deep channels which limit ion depletion near the channel ends during IEF focusing. Ongoing tests are being performed using the lower-density 10-channel arrays to explicitly evaluate repeatability before moving forward to comparative analyses using high-density arrays.

Task 4– System Demonstration

Following optimization of the MS^3 system using *E. coli* cell lysates, full demonstration of the technology using *H. pylori* as the validation model was to be performed in Task 4. Due to the difficulties encountered in achieving acceptable reproducibility of the system using *E. coli*, Task 4 was not initiated. Ultimately, the goal of developing a parallel high density two-dimensional microfluidic protein separation platform could not be completed within the timeframe allocated for this Phase II project. However, proof-of-concept for the separation platform has been provided, and the key challenges for improving system performance have been identified. Efforts were made to expand upon the low-density proof-of-concept platform and develop a higher density two-dimensional microfluidic platform capable of providing the peak capacity required to produce complex PEMs to be used for the detection of biological warfare agents. It should be noted that the highly coupled and parallel microfluidic platform developed here raised a number of unique challenges which proved to be significantly more difficult to address when compared with other microfluidic bioseparation platforms developed by our team and reported by other groups. As a result, many of the issues that prevented all of the project milestones from being met could not be foreseen and/or resolved within the award period. Work on this project is ongoing using internal research funds at Calibrant.